Lasers in Manufacturing Conference 2021

Metallurgy of dissimilar laser beam welded lap joints of supra-ductile and ultra-high strength steels

Martin Dahmen[a,*], Berkan Deniz[a], Dirk Petring[a]

[a]*Fraunhofer Institute for Laser Technology,Steinbachstrasse 15,5074 Aachen, Grmany*

Abstract

Results of research on laser beam welding of a high manganese X30MnCrN16-14 (1.4678) to a press hardened X46Cr13 (1.4304), a dual phase steel (1.0944), and a press-hardened manganese boron steel (1.5528) in lap joint configuration will be reported. A pre-assessment of the local mechanical properties by micro hardness measurements revealed their uneven distribution over the weld zone. Based on metallographic inspection the underlying microstructures were revealed. By EDS analyses the local alloy constitutions were determined and assed by of COHMS diagrams. It was confirmed that in the combination with the high manganese steel the formation of ferritic phases, ferrite is largely suppressed to the favor of austenite and α' and ε martensite. These findings were in part confirmed by nano indentation. The results allow an insight into the properties linked to melt transport but indicate some further research.

Keywords: Metallurgy; High manganese steels; dissimilar welding; microstructure; phases

1. Introduction

Ever increasing demands of the manufacturing industries on material and resource efficiency forced the development of new steel grades materials with increased strengths and improved properties, ultra-high strength and supra-ductile steels alloyed with manganese. Since the development of manganese steels by Hadfield in 1882, questions have been raised about their weldability. It was only with the development of low carbon steels, the possibility of producing sheets and an increasing interest of the sheet metal processing industry that grades suitable for welding were also developed. With the further development of these materials, the first attempts at laser beam welding followed. The latter process is considered a suitable tool

* Corresponding author
E-mail address: martin.dahmen@ilt.fraunhofer.de.

for welding dissimilar joints in lap joints due to the concentrated energy input, the low heat input into the workpiece and the welding of complicated seam geometries. The need to join these high manganese steels with dissimilar grades has led to strengthening research efforts. Schaeffler diagrams have been extended and new constitutional diagrams postulated by scientists for this class of alloys, which continue to allow prediction of the properties of welded joints. Currently, the focus of research is on the further development of weldability with different processes as well as on the determination of the mechanical-technological properties of such joints.

Welding trials were undertaken in order to deeper understand the flow patterns and the resulting intermixing of materials in dissimilar laser beam welding of lap joints. In a metallographic study the micro-structure of the re-solidified weld material was studied at cross-sections by metallographic inspection. Hardness scans are used to attain a clearer picture of the phases of the micro-structure. This paper deals with an investigation in the lap joint of welded dissimilar plates - the determination of the mixing in the joint plane and the resulting phases as well as their distribution. Depending on the materials in a combination, a number of phases with different mechanical properties are formed, which influence the global properties of the welded joint. In this subject area, the aim of this work is to investigate the influence of beam shaping in connection with the parameters feed rate and beam power on the intermixing and to derive properties of the welds.

2. State of the art

Mújica Roncery, Theisen, and Weber, 2012 focused their work on the welding of TWIP steels in dissimilar and dissimilar joints. The manganese loss, the degree of intermixing with low-alloy steels and segregation in the welds were investigated. In dissimilar compounds, areas with lower manganese content are formed, which lead to the formation of martensite. Due to micro-segregation, manganese and carbon accumulations (Rossini et al. 2015) occur in the inter-dendritic zones during solidification.

Dahmen, Daamen and Hirt, 2014 investigated two high manganese steels with different carbon contents. Both samples were produced in butt joint and solidified in an austenitic microstructure. A manganese loss of one wt.% was determined in the weld. In addition, the hardness results showed that the grade with the higher carbon content experienced a drop in hardness in the weld.

Behm et al. 2014 demonstrated welding of a TWIP steel in dissimilar joints with a two unalloyed steels at constant laser power and varying speed in overlap. Martensitic phases occurred, which were dependent on the degree of mixing of the two materials. Among the dissimilar joints, the joint with the highest austenite content had the highest measured shear force. Nevertheless, the strength in the shear tensile test of the dissimilar compounds was lower than that of the weakest dissimilar compounds.

Investigations by Dahmen, Lindner, and Monfort, 2016 and Damen, Lindner, and Petring, 2017 on dissimilar joints in the butt joint between a TWIP steel (1.4678) with a metastable austenitic (1.4301) and a stainless martensitic steel (1.4034) led to crack-free welds during joining to medium gauge sheet steel. Both compounds solidify austenitically with small martensitic phases in regions with increased carbon content. The same species solidifies dendritically, while in the dissimilar compound stem-like grains with a dendritic substructure can be seen. In conjunction with the martensitic stainless steel, equiaxed grains were detected in the centre of the weld zone. Due to the low thermal conductivity of the TWIP steel, a small heat-affected zone is created. Thermal treatment to improve mechanical properties is recommended for dissimilar joints with martensitic stainless steels.

During investigations by Lun et al, 2017 a medium manganese TRIP steel was joined in similar and dissimilar welded to both, a dual phase steel and a high-strength low-alloy steel, by square butt welds. The dissimilar TRIP steel solidified in the weld predominantly martensitic with a small amount of austenite between the

dendrites, which prevented martensite formation due to micro-segregation of Mn and C. The welds associated with the dual phase steel and low alloy steel solidified martensitic. While the similar joint showed no softening of the heat-affected zone, the combination with the dual-phase steel showed the highest hardness in the weld but also softening due to tempering of the martensite. It was demonstrated that the softening of the HAZ can be described as a function of heat input and martensite content in the base metal. Fractures were detected in tensile specimens in the base material of the DP980 and the low-alloy steel, while in the similar joint the fracture occurs in the tempering zone.

To predict microstructure and properties of dissimilar welds between high manganese steels and other grades (Wittig et al. 2017a, 2017b, 2019a, 2019b) created a constitution diagram called "Constitution of High Manganese Steel Welds" (COHMS). Constructed under real welding conditions using a conventional arc welding process the prediction accuracy in terms of microstructure is about 93 %. Specimens were heated to the molten phase and then cooled. Unlike conventional Schaeffler diagram, in the COHMS diagram two types of martensite (ε and α') are taken into consideration. In laser deep penetration welding, higher energy densities and faster cooling rates prevail than in conventional arc welding. Dedicated analysis has shown that the cooling rates exert minor effects on the microstructure. As possible reason the high content of manganese and carbon were assumed which contribute to the reduction of the critical cooling rate.

3. Experimental

3.1. Materials

At the center of the investigations stand a stainless high-manganese steel X30MnCrN16-14 (material number 1.4678) with a fully austenitic microstructure. The material was cold rolled to a yield strength of 1 GPa. After welding the strength in the fused zone is lost resulting in an austenitic microstructure with a yield strength of 500 MPa. This material was welded to three ultra-high strength steels. The first partner is a stainless chromium steel X46Cr13 (1.4034), comparable to a carbon-rich A420, press-hardened to a yield strength of 1.2 GPa with a martensitic-austenitic microstructure. Second, an also press-hardened manganese-boron steel 22MnB5 (1.5528) with a tensile strength of 1.5 GPa and a fully martensitic microstructure.

Table 1. Alloy compositions of the materials in mass percent

Material	Designation	C	Si	Mn	Cr	Ni	Cu	N	Others
1.4678	X30MnCrN16-14	0.3	-	16	14	0.2	0.5	0.3	-
1.4034	X46Cr13	0.46	0.33	0.72	13.8	0.32	0.11	-	-
1.5528	22MnB5	0.25	0.40	1.35	0.25	-	-	0.01	Al, V, B, Ti,

Table 1 contains the chemical composition of the materials under investigation.

3.2. Welding trials

Parallel lap welds have been performed with welding speeds 3, 7, and 10 m/min with the beam power adjusted to attain a sufficient full penetration. Also, the focusing condition have ben varied using two focal lengths (280 and 600 mm) at a wavelength of 1030 nm. Also the layer sequence was changes in order to assess the effect of the position of either material in the system on the resulting mixture in the fused zone.

3.3. Inspection and assessment

The inspection focuses on the fused zone with the main interest to identify its local microstructure and local chemical composition. Macro sections have been used to identify the outer shape of the welds and the dimensions of the seam. For contrasting a set of etchants has been used enabling the clarification of the solidification structure which gives a picture of the underlying flow prior to solidification. Depending on the combination of materials these reagents were used either as single etches or coupled etches using a sequence of two etchants. All etches have been carried out at room temperature.

Table 2. Etchants used in metallographical inspection

Name	Composition	Duration	Etching effects
Nital 3%	3ml HNO_3 100ml C_2H_5OH	3 – 10 s	Grain boundary etch ono ferrite
Vilella	5ml HCl 2g Picric acid 100ml C_2H_5OH	12 s	Macro etch, grain size and grain boundaries, martensite, ferrite, and carbides
Lichtenegger und Bloech, variation	200ml H_2O 20g NH_4HF_2 2g $K_2S_2O_5$	14 -30 s	Austenite: blue, grey Martensite: brown, grey Ferrite: white, beige Carbides: white

Phase discrimination has been carried out by metallographic inspections at microsections with magnifications up to 500 using an optical microscope. Special emphasis was put on the phases austenite, bainite, carbides, ferrite, and the two variations of martensite ε and α'.

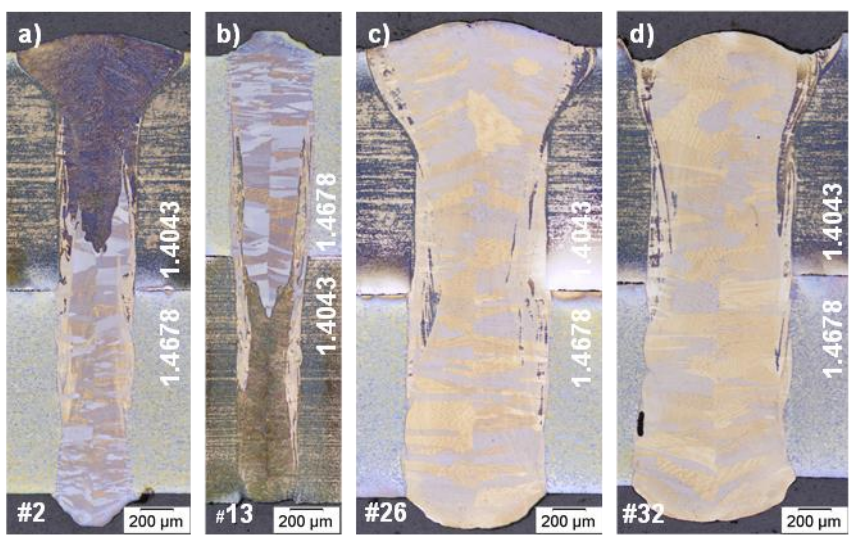

Fig. 1. Macro-sections of dissimilar welds in the combination 1.4678 and 1.4034: Left f = 280 mm at 4 (a) and 10 m/min (b) welding speed, right f = 600 mm at 7 (c) and 10 m/min (d)

For further phase determination hardness measurements in a distance of 0.2 mm above and below the fusion plane, Vickers with a test load of 0.2 kp (1.96 N) were conducted. Measurement tracks have been

conducted transverse the seam cross-section obeying the rule of three-fold diagonal distance between the indentations. As a typical value a distance of 90 µm was set. EDS measurements at locations coinciding the hardness indentations in order to attain an assignment of the hardness values at these locations. Calculating the equivalents for chromium and nickel using the formula of Wittig et al. 2017b and inserting the data into an unaltered COHMS diagram, for confirmation of the data, but also for testing the limits of this type of diagram.

4. Results

4.1. Seam shape and intermixing

Focusing conditions and welding speed affect the seam shape. Fig 1 show macro-sections of four different welds in the combination of 1.4678 and 1.4034. The cross sections shown on the left-hand side are welded with a focal length of 280 mm at welding speeds of 4 and 10 m/min and a beam power of 2.2 and 5.8 kW, respectively. On the right-hand side seams welded with a long focal length of 600 mm with a speed of 7 and 10 m/min at beam powers of 5.6 and 7.8 mm, respectively. For the slower speed setting the seam has a nail shape whereas for the higher speed the shape becomes more rectangular.

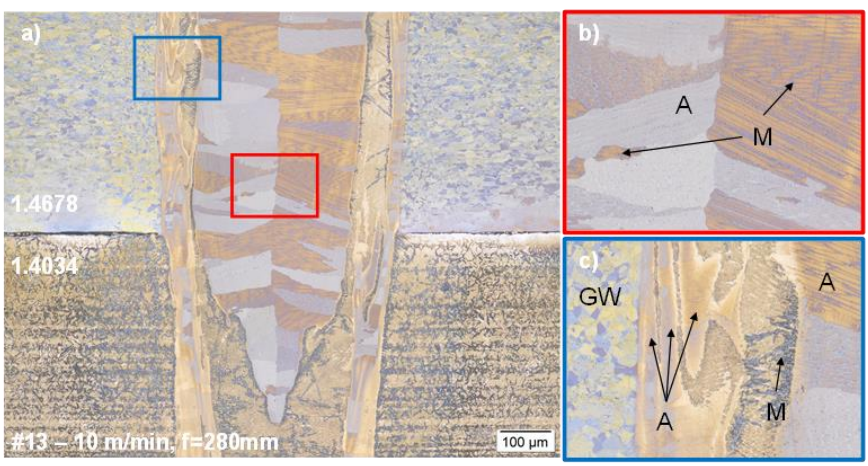

Fig. 2. Microstructure in the vicinity of the fusion plane in the combination 1.4678 and 1.4034

This holds true for all other combinations in any order of layer. It can be also observed that there is a clear distinction in the upper and the lower part of the former fused zone in the welds produced under the shorter focal length. There is a martensitic region concentrated at the level of 1.4034 and a predominant austenitic microstructure seen at the level of the 1.4678. If welded at the long focal length of 600 mm the core of the fused zone becomes more homogenously mixed. In all welds there is a layer of mixing streaks visible in the regions adjacent to the fusion lines.

4.2. Microstructure

Microstructure analysis has been carried out in the vicinity of the fusion plane in order to obtain information of the occurrence and distribution of phases in this critical area.

Fig 2 shows photographs of metallographic etchings of a weld between 1.4678 and 1.4304 where the high-manganese steel is in top position obtained by tint etching. The seam was welded with at 10 m/min using the short wavelength of 280 mm. The photograph shows a limited intermixing by distinguishable zones at the weld centre line and the fusion line (Fig 2a). The solidification mode is predominantly austenitic. The the mainly austenitic structure of central region indicates a downward flow of the high-manganese material in the place of the section, as shown in Fig 2b). There are some martensitic islands in the interdendritic regions. Adjacent to the fusion lines dominates an upward flow, detectable from the increased content of martensite in these regions. This martensite occurs in mixing streaks and are characterized by the blueish colour in the tint etching. An increased intermixing effect can be concluded from the presence of vortex-like structures in this area.

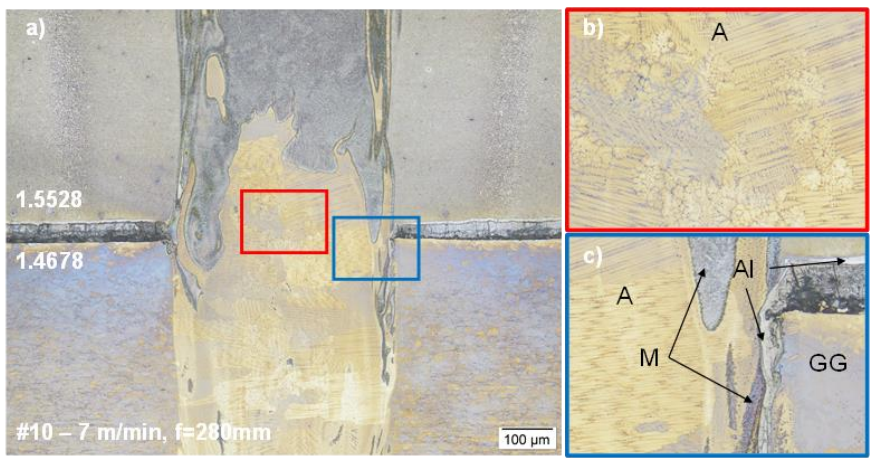

Fig. 3. Microstructure in the vicinity of the fusion plane in the combination 1.4678 and 1.5528

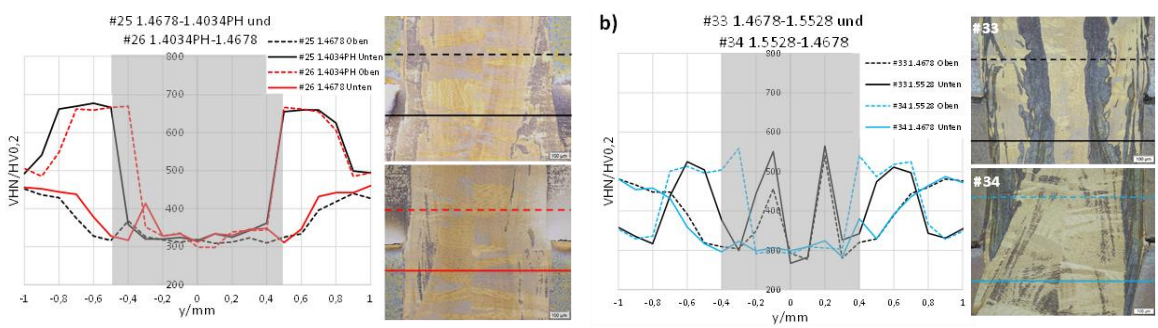

a) Combination 1.4678 and 1.4034

b) Combination 1.4678 and 1.5528

Fig. 4. Micro-hardness measurements across the seam in different layer sequences

Fig. 3 shows photographs of metallographic etchings of a weld between 1.4678 and 1.5528 where the high-manganese steel is in lower position obtained by tint etching. The scale-protection layer of aluminium-silcion alloy was left on the surface of the manganese-boron steel in order to trace the melt flow at the fusion lines. In the centre region an austenitic microstructure is dominant whereas in the regions adjacent to the fusion lines “horns” of martensite become visible. Also in this case the boundary regions show a limited intermixing in vortex-like streaks. The deflection of the aluminium-silicon layer towards the lower part of the weld indicating a strong downward flow in this region.

4.3. Hardness

Hardness plots of welds in the different combinations are shown in Fig 4. Besides the material combination the layer sequence was changes. The weld region is located at the centre and ranges from y ≈ -0.4 mm to y ≈ 0.4 mm. The welds have been conducted using a focal length of 600 mm with a welding speed of 7 m/min. The hardness curve in Fig 4a indicates a fully austenitic microstructure in the fused zone. Hardness and strength respectively are on the level of the solution annealed high-manganese steel. 1.4678. As intermixing is more pronounced in the welds conducted with the long focal length it is assumed that the resulting manganese content is still sufficient to suppress martensite formation.

Fig 4b shows the hardness distribution in a weld of the combination with 1.5528. The low-alloyed character of this material leads to a different appearance of the microstructural distribution. The hardness curve shows strong oscillations ranging from the low value of 300 HV0.2, indicating the presence of austenite to peak values of 550 HV0.2 of a martensitic or bainitic structure. The metallographic section at the right-hand side of the figure show the co-ordinated distribution of the structural components, brown-grey for the austenite and blue-grey for martensite.

4.4. EDS analysis and COHMS diagrams

Fig 5 and 6 show the results of EDS measurements across the fused zone of the weld and the corresponding representation of the results in the COHMS diagram. All heavy elements were measured, the light elements carbon and nitrogen were calculated using chromium and manganese, respectively, as tracers.

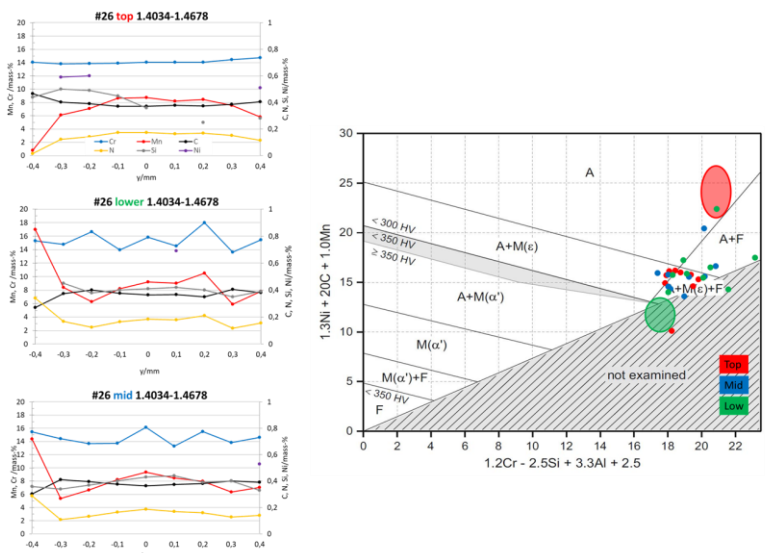

Fig. 5. Results of EDS measurements from a weld in the combination 1.4678 and 1.4034 measurements and their representation in the COHMS diagram

The distribution of elements in the combination with 1.4034 is shown in Fig 5. Due to stronger intermixing it appears as more or less constant with manganese levels around 8 mass-percent in average. Still high concentraions of nitrogen and carbon (0.15 and 0.4, respectively) lead to a predominantly austenitic microstructure in the weld. In the COHMS diagram the chromium and nickel equivalents calculated from the

measurement results predict a microstructure in the austenitic (A), partially with ε-martensite (a+M(ε)), but also in the austenitic-ferritic (A+F) regions. Epsilon martensite was not detected during the metallographic inspection. Also no ferrite in this combination was found in this combination for all welding parameters. A reason for this inaccuracy is assumed that the COHMS diagrams were developed for the combination of high-manganese and un- or low-alloyed steels. The high chromium content in the 1.4034 needs some fitting the boundary lines in the diagram in this case.

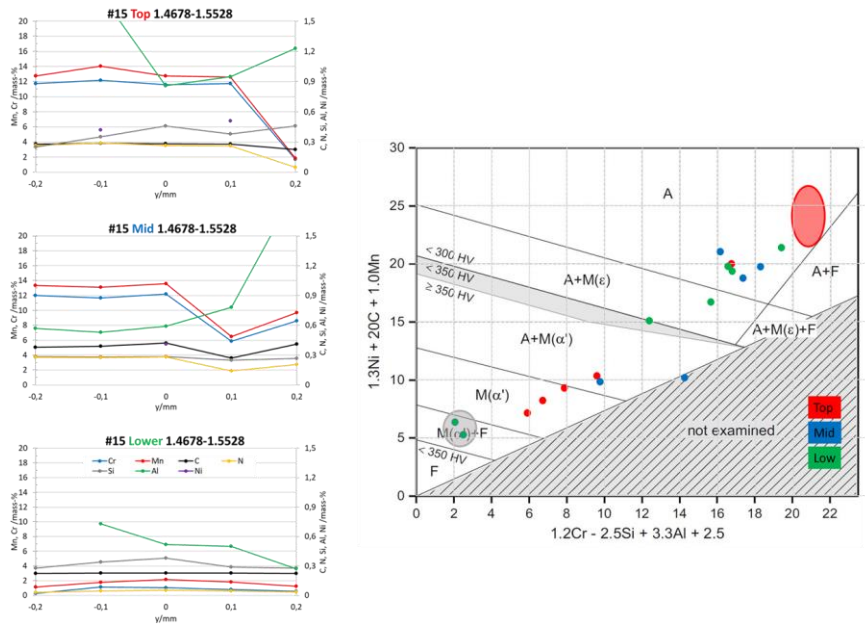

Fig. 6. Results of EDS measurements from a weld in the combination 1.4678 and 1.5528measurements and their representation in the COHMS diagram

Results of EDS measurements for the combination with the manganese-boron steel 1.5528 are displayed in Fig 6. The distribution of the elements shows more limited intermixing of the material, especially in the upper and mid part of the fused zone. High manganese contents will lead to a austenitic structure. The lower part is characterized by low manganese contents. Here, the pre-dominance of a martensitic microstructure is expected. Transforming the results to chromium and nickel equivalents and displacing them in the COHMS diagram confirms the presence of austenite in regions with high manganese content and the martensitic one in regions with low manganese.

5. Conclusions

Results of welding trials of dissimilar welds of a stainless high-manganese steel 1.4678 in combinations with a press hardened lean chromium steel 1.4034 on the on hand and a press-hardened manganese-boron steel 1.5528 are presented. The results show a limited intermixing of the either materials when welded with a beam shaping using a focal length of 280 mm resulting in a clear distinction in a upper and lower zone of the weld where the either alloy constitutions dominate. Welding using a focal length of 600 mm leads to a more homogenous phase distribution in the core of the fused zone and some limited mixing along the fusion

boundaries. Shorter duration of the system in the liquid phase in the case of the shorter focal length are assumed to be the cause. In the combination with the 1.4034 the microstructure in the weld appears predominantly austenitic caused by high manganese, carbon and nitrogen contents. In the COHMS diagram this leads to a concentration of the chromium and nickel equivalents in the austenitic region. Welding the low-alloyed 1.5528 to the high-manganese steel leads to a more layered microstructure in the weld zone. These layers consist of either austenite, martensite, or mixtures of both phases. Consequently, the display int the COHMS diagram scatters over the complete range of possible phases. This was confirmed by detailed microstructural analysis as well as by hardness measurements. The results can serve as a basis for a deeper understanding of the flow patterns underlying the welding process, but can also give rise to an understanding of the mechanical behavior of the weld zone under load.

Acknowledgements

The research project IFG 19556 N / FOSTA-P-1175 "Weiterentwicklung, fügetechnische Absicherung und technische Auslegung von Schweißverbindungen mit martensitischen Chromstählen" from the Research Association for steel Application (FOSTA), Düsseldorf, was supported by the Federal Ministry of Economic Affairs and Energy through the German Federation of Industrial Research Associations (AiF) as part of the programme for promoting industrial cooperative research (IGF) on the basis of a decision by the German Bundestag. The project was carried out at Fraunhofer Institute for Laser Technology, Research group System Reliability, Adaptive Structures, and Machine Acoustics of Darmstadt Technical University, and Laboratory for Material and Joining Technology of Paderborn University.

References

Behm V, Höfemann M, Hatscher A, Springer, A, 2014. Investigations on Laser Beam Welding Dissimilar Material Combinations of Austenitic High Manganese (FeMn) and Ferrite Steels. Physics Procedia 56: 610 – 619

Dahmen M, Daamen M, Hirt G, 2014. Laser beam welding of high manganese TWIP steels produced by twin roll strip casting. 2nd International Conference on High Manganese Steel, Aachen, August 31st – September 4th, Aachen

Dahmen M, Lindner S, Monfort D, Petring, D, 2016. Weld Metallurgy and Mechanical Properties of High Manganese Ultra-high Strength Steel Dissimilar Welds. Physics Procedia 83: 344 – 351

Dahmen M, Lindner S, Petring D, 2017. Perspectives of laser-beam welding of ultra-high steels. WLT Conference on Lasers in Manufacturing, München; June 26th-29th, 2017 Paper ID 251

Lun N, Saha DC, Macwan A et al, 2017. Microstructure and mechanical properties of fibre laser welded medium manganese TRIP steel. Materials & Design 131: 450 – 459

Mújica Roncery L, Weber S, Theisen W., 2012. Welding of twinning-induced plasticity steels. Scripta Materialia 66: 997 – 1001

Rossini M, Spena PR, Cortese L et al., 2015. Investigation on dissimilar laser welding of advanced high strength steel sheets for the automotive industry. Materials Science and Engineering: A; 628: 288 – 296

Wittig B, Zinke M, Jüttner S, Keil, D, 2019a. A new constitution diagram for dissimilar metal welds of high-manganese steels. Welding in the World; 63: 491 – 499

Wittig B, Zinke M, Jüttner S, Keil D, 2017a. Einfluss der Aufmischung auf das Mischschweißgut hochmanganhaltiger Stähle. DVS-Berichte, Vol. 365, 247-255

Wittig B, Zinke M, Jüttner S, Keil D, 2017b. Experimental simulation of dissimilar weld metal of high manganese steels by arc melting technique. Weld in the World 2017; 61: 249 – 256

Wittig B, Zinke M, Jüttner S, 2019b. Martensite formation in dissimilar weld metals of high-Mn steels. The 4th International Conference on Medium and High Manganese Steels: April 1-3, 2019, Aachen, Germany, Extended Abstracts 378